Visual Abstract

Couple effects of temperature and fatigue, creep-fatigue interaction and thermo-mechanical loading conditions on crack growth rate of nickel-based alloy

Valery Shlyannikov
FRC Kazan Scientific Center of Russian Academy of Sciences, Russia
shlyannikov@mail.ru, http://orcid.org/0000-0003-2468-9300

Aleksandr Inozemtsev, Aleksey Ratchiev
JSC "UEC-Aviadvigatel", Russia
impex@avid.ru, ratchiev@avid.ru

ABSTRACT. The ambient and high-temperature fatigue crack growth behaviors in C(T) and SENT specimens of Ni-based superalloy for turbine disk application were studied in a wide interval of temperatures 25–750°C using a combination a electro- and servohydraulic test systems and fractographic investigations. The fatigue, creep-fatigue interaction and thermo-mechanical in-phase fatigue (TMF IP) crack growth tests are performed under isothermal and dynamic waveforms loading conditions. The interpretation of the experimental results is given in terms of the traditional stress intensity factors and C-integral as well as new normalized cyclic fracture diagrams. It is found that there are definite temperature-sensitive regions separate for harmonic fatigue and creep-fatigue interaction loading conditions in which the crack growth rate of Ni-based alloy increases sharply. Scanning electron microscopy in longitudinal sections containing cracks revealed the mechanisms responsible for fatigue crack initiation and growth. The couple effect of temperature ranging and isothermal and dynamic waveforms loading conditions on fatigue life was discussed.

KEYWORDS. Crack growth rate; Elevated temperature; Fracture resistance parameter; Nickel-based alloy.

OPEN ACCESS

Citation: Shlyannikov, V., Inozemtsev, A., Couple effects of temperature and fatigue, creep-fatigue interaction and thermo-mechanical loading conditions on crack growth rate of nickel-based alloy, Frattura ed Integrità Strutturale, 61 (2022) 46-58.

Received: 21.03.2022
Accepted: 08.04.2022
Online first: 14.04.2022
Published: 01.07.2022

INTRODUCTION

Nickel-based superalloys have been successfully used in aero engines for decades. High-pressure compressor and turbine discs of modern engines in the rim region experience prolonged stress at high temperatures (500–700°C) in an oxidizing environment. Time-dependent intergranular cracking may occur under such conditions and

contribute to accelerated cyclic crack growth rates during service operation. Several studies have been published for materials ranging from early Fe–Ni-based alloys, some alloys originally developed for cast turbine blades, to recent powder metallurgy processed alloys [1–10]. Together with the trend of alloy development towards alloys containing a high volume fraction of γ', the potential susceptibility to accelerated, environmentally related cracking has increased [11].
Such an increase in efficiency of the gas turbine is usually achieved either by weight reductions or by increasing the combustion temperature as a result of fuel being burnt at temperatures approaching the stoichiometric value [12]. In either case, the material choice is of critical importance. Effectively, the modern criteria for selecting materials include requirements on high temperature fatigue and creep capabilities, as well as requirements on suitable environmental and corrosion resistant properties, which in the present context typically results in the employment of nickel base superalloys. The motivation of these strict criteria is that the gas turbine operation cycle imposes harsh alternating mechanical and thermal loads on the material during start up, take off, descent and shut down. A complex failure mechanism, caused by combined thermal and mechanical load cycles is the primary life limiting aspect for many engineering components exposed to elevated temperatures, such as parts in the combustion chamber, along with turbine blades and discs elevated temperatures, such as parts in the combustion chamber, along with turbine blades and discs [13].
The crack growth behaviour is often simulated in the laboratory by the application of a dwell fatigue loading waveform or pure sustained loading. Therefore, the aim of this study is to provide interpretation and comparison of a range of isothermal and non-isothermal experimental crack growth data generated by three type tests carrying out by stress-controlled pure fatigue, creep-fatigue interaction and in-phase (IP) and thermo-mechanical fatigue (TMF) conditions. The ordering of the crack growth rate curves is supported by detailed fractographic analysis which shows intergranular or transgranular crack growth in test C(T) and SENT specimens depending on thermo-mechanical fatigue conditions. Subject for experimental studies at elevated temperatures is Ni-based superalloy which is widely used in the production of aviation gas turbine engine discs.

TEST EQUIPMENT AND LOADING CONDITIONS

The specimen geometry designed for the pure fatigue and creep and fatigue interaction tests is the most popular in experimental fracture mechanics pure mode I C(T) specimen (Fig. 1a). Its dimensions basically follow the ASTM standard [14] with a thickness is 10 mm and a width is 40 mm. For the thermo-mechanical in-phase fatigue loading conditions, the single edge notched tension (SENT) specimens were employed [15]. The specimen geometry is displayed in Fig. 1b. The grip section of the specimen was cylindrical with a diameter of 22 mm while the middle section had an approximately rectangular cross section with a thickness of 7 mm and a width of 20 mm. The specimens were manufactured through turning and wire electrical discharge machining, without application of any additional surface finishing process.

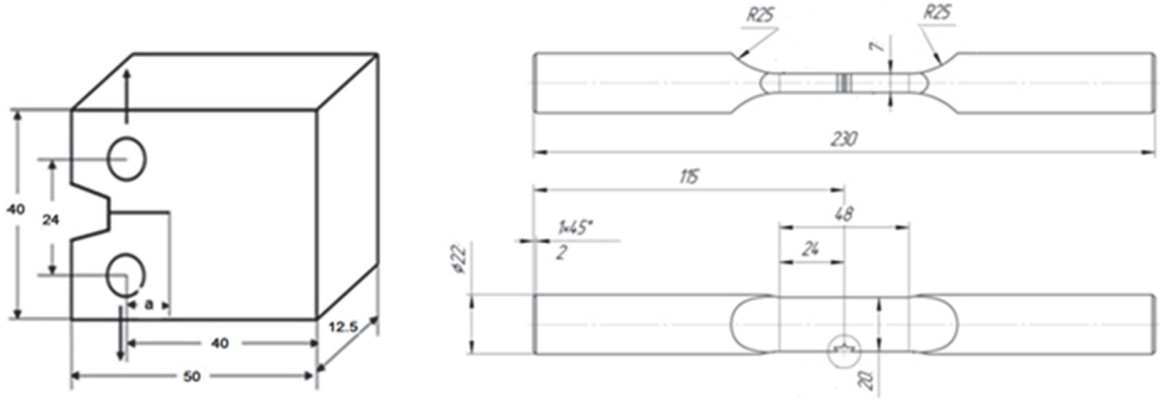

a) b)

Figure 1: Compact tension (a) and single edge notched tension (b) specimens used for the creep-fatigue and TMF crack growth experiments.

Pure harmonic fatigue and thermo-mechanical fatigue in-phase (TMF IF) tests and pre crack operations were conducted in a Zwick/Roell HA100 servo hydraulic test machine equipped with an induction heating system including a cylindrical copper coil with its centre axis coinciding with the specimen centre axis. To even out the temperature distribution and

assist cooling, compressed air flow directed towards the specimen through three nozzles was used, positioned circumferentially with equal angular spacing and the same distance to the specimen, as well as at the same vertical position as the notch. All tests were controlled and monitored using a dedicated TMF software, which automatically performs a pre test procedure, involving thermal stabilisation, thermal strain measurement and validation. The Zwick/Roell HA100 setup is displayed in Fig. 2. The creep–fatigue interaction tests were performed on the test stand of UTS-110MH-5-0U equipped by highprecision crack opening displacement extensometer and a high-temperature three-zone oven (Fig. 3).

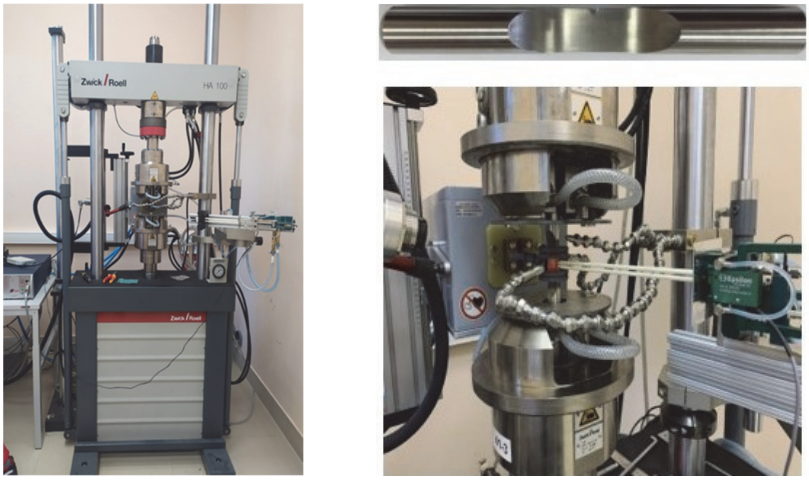

Figure 2: Pure fatigue and thermo-mechanical fatigue test equipment.

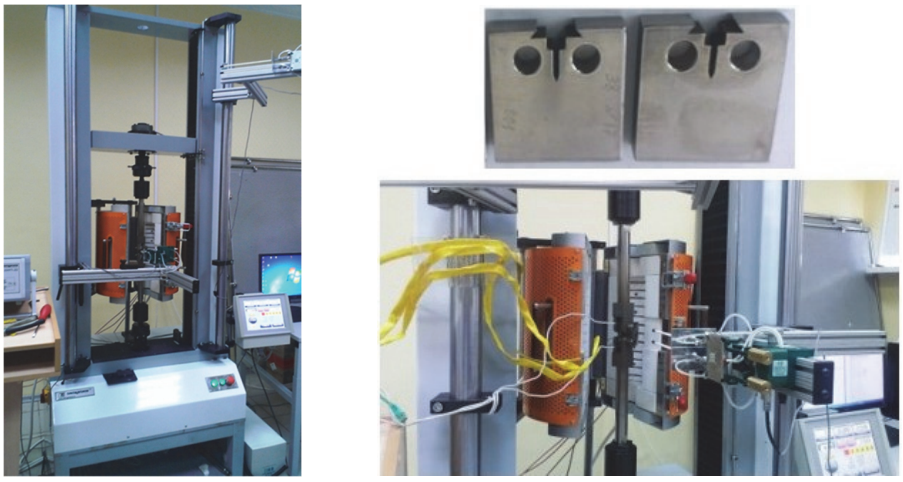

Figure 3: Creep-fatigue interaction test equipment.

This study presents interpretation and evaluation of a range of isothermal and non-isothermal experimental crack growth data generated by four type tests carrying out by stress-controlled fast and slow harmonic fatigue, creep-fatigue interaction and in-phase (IP) thermo-mechanical fatigue (TMF) conditions as it shown in Fig. 4.

Tests on both C(T) and SENT specimens are carried out under loads sufficiently below the yield stress of Ni-based alloy with an initial fatigue crack obtained at room temperature. The pure fatigue tests were performed at ambient 23˚C and elevated temperature 150˚C, 650˚C and 750˚C with an applied nominal stress asymmetry ratio of R = 0.1 under sinusoidal harmonic loading at a frequency of 1.0 and 10.0 Hz. The creep–fatigue interaction crack growth rate tests were carried out at elevated temperature 450˚C, 550˚C, 650˚C and 750˚C with the same stress asymmetry ratio of R = 0.1 in a specially designed the trapezoidal cycle program with the 5-s loading and unloading parts and dwell time of 120 s, which was applied at the maximum load, as can be seen in Fig. 4. The TMF in-phase test parameters employed for the single edge notched specimen is a triangle waveform with asymmetry ratio of R = 0.1 at a loading frequency 0.014Hz over a 400-650°C temperature range with heating and cooling rates at 10°C/s.

During the thermo-mechanical in-phase test in order to employment the unloading compliance method for the crack size determination, direct measurements of the load-line displacement were carried out using capacitive high-temperature strain gauges. The most convenient methods for investigating crack growth at high temperatures, such as the potential drop (PD) methods, was used to measure the current crack size under the fatigue and creep–fatigue types of loading. To fix the intermediate between the precrack and the final crack front positions on the surface of the fractured specimen, the value of the load ratio was changed from R = 0.1 to R = 0.5 twice during the total fatigue life. In this case, the maximum load corresponded to the previous cycle, and the minimum load increased to R = 0.5. This loading change was maintained for 1 min; after that, the specimen was returned to conventional fatigue or creep–fatigue trapezoidal waveform loading conditions with R = 0.1. For each crack front position on the specimen fracture surface, crack sizes at the midplane section a_{mp} and on the outer surface a_{fs} are measured by using of an optical microscope.

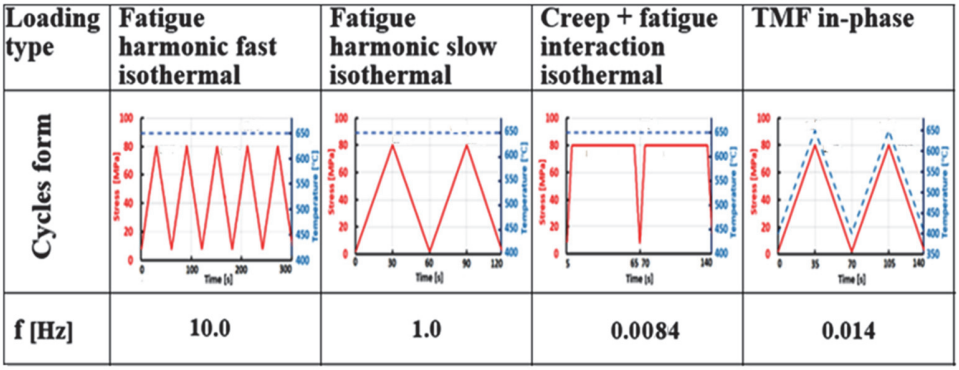

Figure 4: Loading profiles for isothermal and non-isothermal temperature cycling.

To calculate the crack size on the creep–fatigue CGR, at the end of each creep–fatigue test, the PD signal was calibrated with the initial and final crack lengths determined at two basic sections of the crack front in the fractured specimens toward the thickness direction. One section is the outer surface of the specimen; the other is a point placed on the mid-thickness line of specimen. The relationship between the PD signal and crack size was assumed to be linear. The crack lengths on the midplane sections and the outer surface of the specimens were calculated according to the following equations:

$$a_{rs}(t)=\left[\left(a_{fs,f}-a_{fs,0}\right)\frac{\left(U(t)-U_0\right)}{U_f-U_0}\right]+a_{fs,0} \tag{1}$$

$$a_{rm}(t)=\left[\left(a_{mp,f}-a_{mp,0}\right)\frac{\left(U(t)-U_0\right)}{U_f-U_0}\right]+a_{mp,0} \tag{2}$$

where $a_{fs,0}$ and $a_{mp,0}$ and $a_{fs,f}$ and $a_{mp,f}$ are the initial and final crack lengths, respectively, and U_0 and U_f are the initial and final PD. According to this practice of the measurements, the CGR and the force-line displacement rate on the outer surface and midplane sections of the C(T) specimens were obtained. Finally, the crack length was converted into crack growth rate data by using the incremental polynomial method, as described in the ASTM 647 appendixes, standard test method for measurement of fatigue crack growth rates [16].

MATERIAL PROPERTIES AND CRACK GROWTH PARAMETERS

The material used in the tests is heat-resistant XH73M nickel-based alloy, which is used for a GTE turbine disk and operates at elevated temperatures with the occurrence of creep conditions. The chemical composition and the main mechanical properties of analyzed material at both the ambient and elevated temperature are summarized in Tab. 1 and Tab. 2, respectively. In Tab. 2 E is Young's modulus, σ_0 is yield stress, σ_u is tensile strength, δ is elongation, ψ is reduction of area, B and n are the Norton creep constant and exponent.

C	Cr	Mo	Al	Ti	Nb	Ni
0.03-0.07	13.0-16.0	2.8-3.2	1.45-1.8	2.35-2.75	1.9-2.2	basis

Table 1: Chemical composition for XH73M alloy.

T [°C]	σ_u [MPa]	σ_0 [MPa]	E [GPa]	δ [%]	ψ [%]	B [1/(MPa*n·hr)]	n
23	1298.25	904.04	215.77	34.94	54.19	-	-
400	1229.53	830.50	192.87	32.31	50.88	$2.5*10^{-11}$	2.50
550	1205.93	836.42	206.18	27.73	30.12	$4.0*10^{-12}$	3.53
650	1079.30	866.05	192.76	10.67	18.35	$2.1*10^{-16}$	4.80
750	839.85	705.46	161.39	8.27	17.90	$4.0*10^{-26}$	8.85

Table 2: Main mechanical static properties for XH73M alloy.

In the present study, the interpretation of experimental results on the CGR in C(T) specimens of nickel-based alloy at high temperatures are presented in terms of the fracture mechanics characteristics for the conditions of elasticity and creep. Traditionally, the experimental data are presented through the creep C-integral and the elastic SIF which for C(T) specimens is given by the ASTM standard [14] as

$$K_1 = \frac{P}{b\sqrt{w}} f_1(a/w) \tag{3}$$

$$f_1(a/w) = \left[\frac{2+a/w}{1-(a/w)^{1.5}}\right]\left[0.866 + 4.64\left(\frac{a}{w}\right) - 13.32\left(\frac{a}{w}\right)^2 + 14.72\left(\frac{a}{w}\right)^3 - 5.6\left(\frac{a}{w}\right)^4\right] \tag{4}$$

where a is the crack length, w is the length of the working area of the specimen, b is the specimen thickness, and P is the applied load. To interpret the data on crack propagation at high temperatures creep-fatigue interaction loading conditions, the method for determining the C^*-integral can be used, which is based on the experimentally measured load-line deflection V_{FL} in the C(T) specimen. The compliance method [14] has been applied in order to determine the force-line displacement rate $\partial V_{FL}/\partial t$. The relationship between compliance and normalized crack size for experimentally measurements made at the load-line for a specimen with a crack subject to constant force, P, are given by the following equation:

$$C_{FL} = \frac{V_{FL}}{P} = \\ = \frac{1}{Eb}\left[\frac{1+a/w}{1-a/w}\right]^2\left[12.163 + 12.219\left(\frac{a}{w}\right) - 20.065\left(\frac{a}{w}\right)^2 - 0.9925\left(\frac{a}{w}\right)^3 + 20.609\left(\frac{a}{w}\right)^4 - 9.9314\left(\frac{a}{w}\right)^5\right] \tag{5}$$

The expression for extending the C^*-integral concept to small-scale creep conditions in the form of the $C(t)$-parameter is described by the equation [14]:

$$C(t) = \frac{P(\partial V_{FL}/\partial t)}{bw}\left(\frac{f'}{f_1}\right) \tag{6}$$

$$f' = \frac{df_1}{d(a/w)} = f_2 + f_3 + f_4 \tag{7}$$

$$f_2(a/w) = \frac{1}{(1-a/w)^{1.5}}\left[0.866 + 4.64\left(\frac{a}{w}\right) - 13.32\left(\frac{a}{w}\right)^2 + 14.72\left(\frac{a}{w}\right)^3 - 5.6\left(\frac{a}{w}\right)^4\right] \tag{8}$$

$$f_3\left(a/w\right)=\frac{\left(2+a/w\right)}{\left(1-a/w\right)^{1.5}}\left[4.64-26.64\left(\frac{a}{w}\right)+44.16\left(\frac{a}{w}\right)^2-22.4\left(\frac{a}{w}\right)^3\right] \tag{9}$$

$$f_4\left(a/w\right)=\frac{1.5\left(2+a/w\right)}{\left(1-a/w\right)^{2.5}}\left[0.866+4.64\left(\frac{a}{w}\right)-13.32\left(\frac{a}{w}\right)^2+14.72\left(\frac{a}{w}\right)^3-5.6\left(\frac{a}{w}\right)^4\right] \tag{10}$$

where $f_1(a/w)$ is the geometry-dependent correction factor and f' is derivative of factor f_1, which is given with mistakes in the original standard [14].

In the case of TMF IF the interpretation of test results on the CGR in SENT specimens of Ni-based alloy at a temperature of 650°C is presented in terms of the elastic stress intensity factor

$$K_1=\frac{P}{bw}f_5\left(a/w\right) \tag{11}$$

$$f_5\left(a/w\right)=\left[\begin{array}{l}5.835\text{-}69.135\left(\frac{a}{w}\right)+403.734\left(\frac{a}{w}\right)^2-1163.407\left(\frac{a}{w}\right)^3+1797.355\left(\frac{a}{w}\right)^4\\-1415.925\left(\frac{a}{w}\right)^5+447.342\left(\frac{a}{w}\right)^6\end{array}\right] \tag{12}$$

In the future, it is assumed that the crack growth rate will be interpreted in terms of phase field fracture parameters.

CRACK GROWTH RATE IN TEMPERATURE RANGE

Typically, the cyclic fracture diagram is represented by the crack growth rate (CGR) coordinates da/dN versus K_I, where N is the accumulated number of loading cycles. The present study focuses on the couple effects of temperature and different type of cyclic loading, therefore it would be useful to compare the fatigue fracture diagrams for the classic harmonic cycle (with constant loading frequency and loading waveform) and trapezoidal cycle with the holding time at a maximum load, and all other factors being equal.

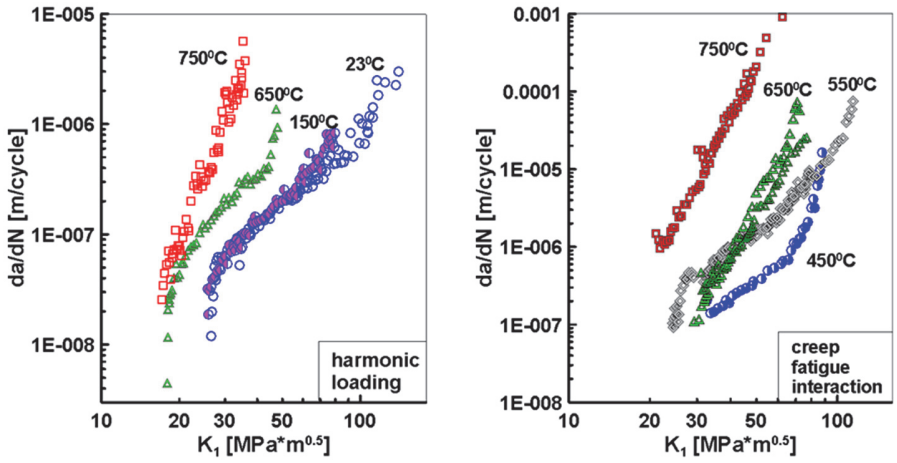

a) b)

Figure 5: Fatigue (a) and creep-fatigue (b) crack growth rate as a function of test temperature.

To this end, Fig. 5a shows the fatigue fracture diagrams of C(T) specimens for a frequency 10 Hz, which were tested at 23°C, 150°C, 650°C and 750°C. For simplicity, the CGR da/dN was set to be dependent on the elastic SIF K_I. A

comparison of these diagrams shows that as the elastic SIF increased, the CGR during the harmonic loading conditions at high temperatures 650°C and 750°C sharp increased with respect to the ambient 23°C and moderately elevated150°C temperatures. Fig. 5b illustrates the creep-fatigue interaction CGR da/dN versus the elastic SIF for the compact specimen as a function of the test temperature ranging between 450°C and 750°C, which consists of the dwell time during 120 sec and 5 sec loading/unloading time, for each loading cycle. Note that the each separate experimental CGR diagram falls within a relatively narrow scatter band. A fairly sharp increase in the crack growth rate is observed during the transition from temperature 650°C to temperature 750°C.

The ASTM E2760 [14] creep-fatigue CGR standard test method recommends presenting the experimental results as a function of the elastic SIF K_I and $C(t)/C^*$-integral. Nevertheless, there are restrictions in the employment of K_I at high temperatures because this fracture characteristic is satisfied only for linear elastic behavior when the size of the nonlinear creep zone around the crack tip is bounded. Therefore, in the representation of creep-fatigue interaction experimental data, Eqs. (5-10) were used for the computational solutions of the creep C^*-integral.

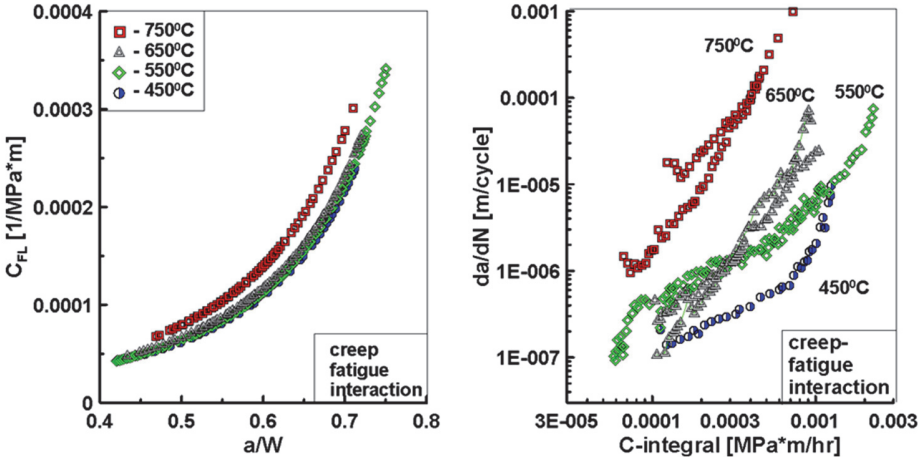

a) b)

Figure 6: Compliance (a) and creep-fatigue crack growth rate as a function C*integral (b) in temperature range.

The calculation of the C*-integral requires the existence of the relationship between compliance (and the associated the force-line displacement rate $\partial V_{FL}/\partial t$) and normalized crack size for experimentally measurements made at the load-line for each tested specimen. In Fig. 6a compliance plotted versus the dimensionless crack length for the Ni-based alloy C(T) specimens at elevated temperatures. It should be noted that the graphs for the temperature range of 450°C-650°C falls within a relatively narrow scatter band, while compliance at a temperature of 750°C increases moderately over the entire range of crack lengths.

Fig. 6b illustrates the creep-fatigue CGR for the Ni-based alloy in the C(T) specimens for a wide range of tested temperatures as a function of the C^*-integral under mode I loading for a creep hold time of 120 s. It was observed that in the contrary to the elastic SIF, the behavior of the cyclic fracture diagrams as a function of the C^*-integral shows the influence of the nonlinear stress-strain rate state at the crack tip. These experimental data clearly show the effect of the dwell time compared with the classical harmonic cycling. In this case, again the crack growth rate sharp increases during the transition from temperature 650°C to temperature 750°C.

Fig. 7a represents a comparison of the behavior of crack growth rate diagrams in terms of the elastic K_I at the same high temperature 650°C for considered thermo-mechanical loading conditions of the C(T) and SENT specimens. As a result of the polycrystalline XH73M nickel-based alloy tests performed, it was found that from the crack growth acceleration point of view, the following order of arrangement of fatigue fracture diagrams is formed: non-isothermal in-phase thermo-mechanical fatigue, isothermal creep-fatigue interaction, isothermal pure slow (f=1 Hz) and fast (f=10 Hz) fatigue. It is noteworthy that in the initial range of values of the stress intensity factor K_I, the crack growth rate for thermo-mechanical in-phase loading is one or two orders of magnitude higher than for other types of loading conditions. The crack growth rate versus K_I during in-phase thermo-mechanical fatigue was significantly higher than during isothermal fatigue at the minimum temperature, even though the advancement of the crack presumably occurs at the same temperature.

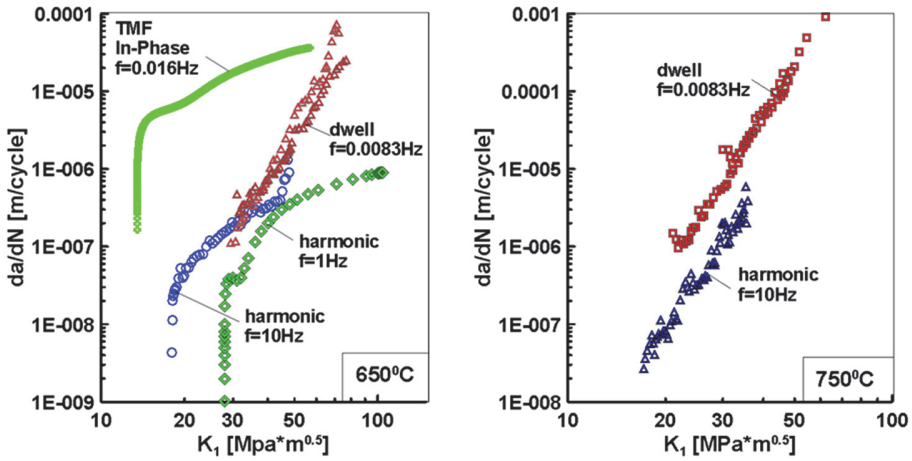

a) b)

Figure 7: Comparison of crack growth rate under different type of loading at 650°C (a) and 750°C (b).

Fig. 7b shows a comparison of the cyclic fracture diagrams as a function the elastic SIF K_I at the highest test temperature 750°C for harmonic (with a frequency 10 Hz) and trapezoidal cycle with the holding time 120 sec at a maximum load. It was observed that creep-fatigue interaction testing produce accelerated crack growth rate compared with pure fatigue due to increased dwell time at elevated temperature. The noted effects of differences in the crack growth rate under harmonic and program loading conditions correspond to known literature data [17].

FRACTURE RESISTANCE PARAMETER BEHAVIOR

Traditionally, the fatigue crack growth rate expressed as a function of the crack-tip stress-intensity factor range, da/dN versus ΔK_I, characterizes a material's resistance to stable crack extension under cyclic loading. This expression yields results that are independent of planar geometry, thereby enabling the exchange and comparison of data obtained from a variety of specimen configurations, loading conditions, and material properties. Moreover, this feature enables da/dN versus ΔK_I data to be utilized in the design and evaluation of engineering structures. In this case, to obtain a rational solution, it is necessary to compare the materials with each other based on their rank of resistance to cyclic failure. Similarly, and in continuation, it is necessary to assess the response of the materials to couple effects of temperature and different type of cyclic loading conditions. At the same time, it should be borne in mind that various types of thermo-mechanical loading determine the use of appropriate fracture resistance parameters such as equivalent SIF, C-integral and creep SIF which is sensitive to damage accumulation and growth [18,19]. The creep-fatigue CGR, which is expressed as a function of the crack-tip SIF or C^*-integral, i.e., da/dN versus K_I, or da/dt versus C^*-integral, characterizes the material property to crack propagation under cyclic loading at elevated temperatures. Such relation must be independent of the cracked body configuration to enable the comparison and exchange of results find out from various combinations of material properties, sample geometries and loading conditions.

For ease of comparison, we restrict ourselves to the well-known Paris law, which describes the linear part of the fatigue fracture diagram

$$\frac{da}{dN} = C\left(\Delta K_1\right)^m \tag{13}$$

where C, m are the Paris constants. This two parameter Paris equation was employment in the present study to describe the relationship between the loading history (frequency, dwell time, temperature) and the crack growth rate, which provides valuable insight into the dominant mechanisms operating at high temperature. In Figs. 5 and 7, crack growth rate diagrams in terms of elastic stress intensity factors K_I, for Ni-based alloys have different scales and ranges of values, thereby making it difficult to compare material behavior for harmonic and creep-fatigue interaction loading conditions at elevated temperature with each other. However, simultaneous two-parameter analyses of the fatigue fracture diagram is difficult and yields an ambiguous estimation of the material crack growth resistance under cyclic loading. Follows to the

authors [20], to overcome these difficulties, it will be convenient to introduce the following dimensionless fracture resistance parameter for the crack growth rate characterization:

$$R_f = \frac{C_T}{C_{amb}} \frac{m_{amb}}{m_T} \tag{14}$$

where C_{amb} and m_{amb} are the CGR Paris law parameters at ambient temperature, C_T and m_T are the CGR Paris law parameters at current value of temperature. Thus, we introduced the non-dimensional variable, which ranged from 0 to 1. The larger this parameter, the greater is the resistance of the material to crack growth under cyclic loading. The larger this parameter, the greater is the resistance of the material to crack growth under cyclic loading. The normalization by the characteristics of the ambient temperature crack growth rate diagram is useful because this type of stress state is the most represented in experimental studies of fracture mechanics. Fig. 8 summarize dependencies the cyclic fracture resistance factor R_f on test temperature for Ni-based alloy in dimensionless form based on Eq.14 for harmonic and creep-fatigue interaction loading conditions. It is found that there are definite temperature-sensitive regions separate for harmonic fatigue and creep-fatigue interaction loading conditions in which the crack growth rate of Ni-based alloy increases sharply. As indicated in Fig. 8, the values of the fatigue crack resistance parameter in terms of R_f change sharply under harmonic loading in the temperature range of about 600°C, whereas under the creep-fatigue interaction, a similar range occurs for temperatures of about 700°C. Thus, the introduced dimensionless parameter made it possible to identify areas of temperature change in which there is a sharp decrease in the resistance of the material to cyclic failure. From the point of view of practical applications, it is important that this parameter separates the conditions of harmonic loading and the creep-fatigue interaction, i.e. the R_f-factor is sensitive to changes in the history of thermo-mechanical loading. In addition, differences in the values of constants C and m in terms of R_f-factor can lead to different predictions of residual fatigue life.

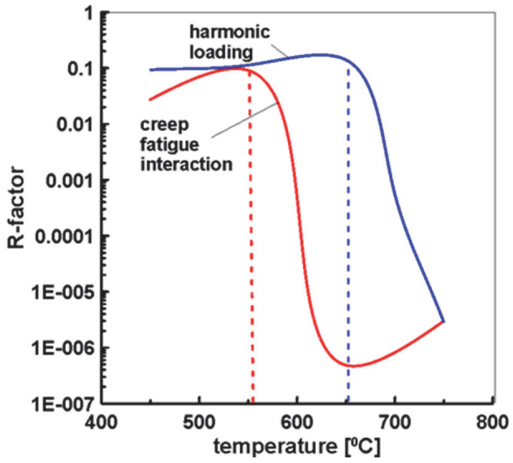

Figure 8: Comparison of cyclic fracture resistance factor behavior in temperature range.

ANALYSIS OF DOMINANT FRACTURE MECHANISM

The following section focuses on comparing the fracture surface characteristics of the investigated specimens that have been tested under harmonic and program loading with temperature variation over a wide range of values by means of a Merlin Zeiss scanning electron microscope (SEM) images. Tab. 3 shows macrostructural images of XH73M Ni-based C(T) test specimens after final failure with crack front positions for the precrack, intermediate, and final crack lengths. It was observed that the shape of the crack front in the specimen changes from the initial rectilinear to essentially curvilinear under the influence of the test temperature. The sensitivity of the fracture surface changes for the experimental initial rectilinear and subsequent curvilinear fronts of growing cracks with progressive tunneling increased as the temperature increased under pure fatigue and creep-fatigue loading conditions. Such behavior is due to tunneling of the crack front which leads to the differences in the crack growth rate in the middle section and free surface of the C(T) specimen as mentioned by the authors [17].

T [°C]	Harmonic fatigue, f = 10 Hz	T [°C]	Creep fatigue interaction, f = 0.0083 Hz
23	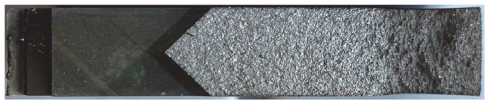	450	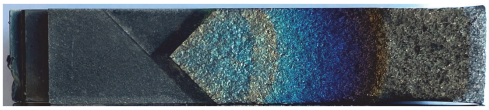
150	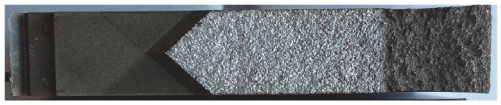	550	
650	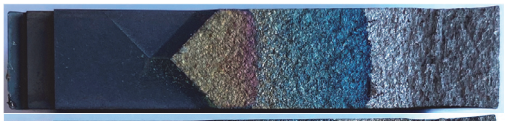	650	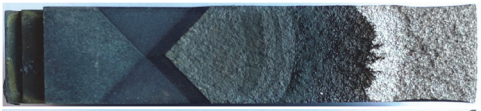
750	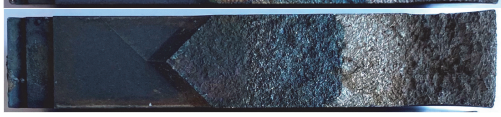	750	

Table 3: Tested specimen fracture surfaces.

The results of the previous section shown in Fig. 7a suggest that crack growth in XH73M nickel-based alloy in the temperature range between 23°C and 750°C under harmonic and creep-fatigue interaction loading conditions is mainly controlled by the deformation caused at the crack tip. Note that, many investigators have pointed out that crack tip oxidation clearly influences the crack growth rate at constant elevated temperature for nickel base superalloys. In particular, it has been convincingly demonstrated that the effect of oxygen accelerates the isothermal crack growth rate by performing tests at different partial pressures of oxygen [21–24]. Clearly, there is a potential influence of material related aspects, such as the couple effects of temperature and thermo-mechanical loading conditions the at the crack tip region, which requires attention in view of the analysis of dominant fracture mechanisms.

Fig. 9 displays a Merlin Zeiss SEM images of the crack path morphology of XH73M nickel-based alloy in the centre of the specimen, i.e. middle position of the crack front, for the pure fatigue test with a frequency of 10 Hz for the temperature range of 23°C-750°C at a crack length of roughly 12 mm in all specimens. In Figs. 9a and 9b fatigue striation formation were observed at the surface of the test C(T) specimens at ambient (23°C) and moderate elevated (150°C) temperature. The relief with fatigue striation is dominant for the entire fracture surface with a gradual increase in the striation spacing with increasing crack length. It can be seen in Figs. 9a and 9b that the fatigue striations in some places of the specimen fracture surface are intersected by plastically deformed slip bands, the number of which increases with increasing test temperature. The fatigue striation spacing approximately correlates with the crack growth rate (see Fig. 5a) and is in the range of spacing $\approx 10^{-8} \div 10^{-6}$ m.

When the test temperature under harmonic loading reached of 650°C and then 750°C, the fracture pattern of XH73M nickel-based alloy changes drastically as it follows from Figs. 9c and 9d. Distinctive features in these SEM images is the general observation of increased tendency for intergranular growth with increasing temperatures under isothermal conditions. It can be assumed, that grain boundary sliding ahead of the crack tip to complement environmentally (temperature) assisted intergranular cracking of considered nickel base superalloy. The crack path morphology analysis, including the mapping oxygen by the Oxford Instruments energy dispersive X-ray spectroscopy, does not indicate a significant distinction regarding the role of oxides between the two test temperatures under harmonic loading with a frequency of f=10.0 Hz. From a comparison of morphologies for temperature ranges of 23°C-150°C and 650°C-750°C, it follows that the change in the dominant fracture mechanism under harmonic loading occurs in the temperature range close to 650°C, as predicted by the behavior of the introduced cyclic fracture resistance parameter R_f in Fig. 8.

Fig. 10 represents a Merlin Zeiss SEM images of the crack path morphology of XH73M nickel-based alloy in the middle position of the crack front, for the isothermal creep-fatigue interaction test with a frequency of 0.0083 Hz for the temperature range of 450°C-750°C at a crack length of roughly 12 mm in all specimens. In Figs. 10a and 10b creep-fatigue striation initiation were observed at the surface of the test C(T) specimens at elevated temperature of 450°C and 550°C. Similar to harmonic loading (Figs. 9a and 9b), the fatigue striations in Figs.10a and 10b in some places of the specimen fracture surface are intersected by plastically deformed slip bands. The striation spacing approximately correlates with the creep-fatigue crack growth rate (see Fig. 5b) and is in the range of spacing $\approx 10^{-7} \div 10^{-5}$m.

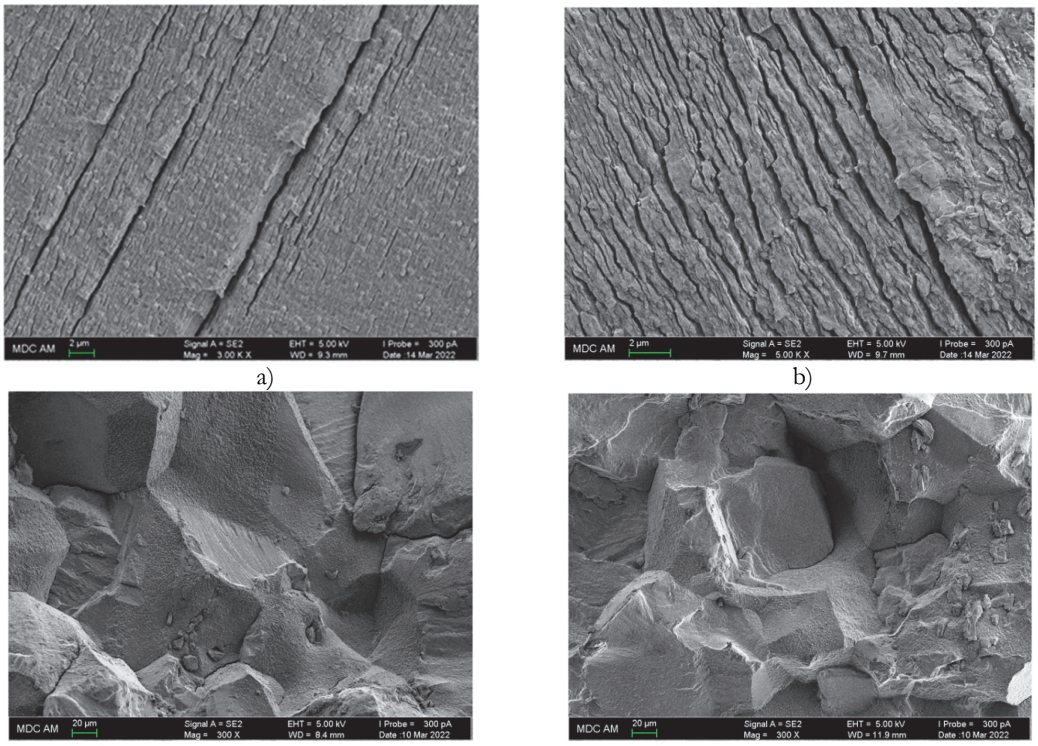

a) b) c) d)

Figure 9: Backscattered SEM images of the crack path morphology for isothermal harmonic fatigue with a frequency of f =10.0 Hz; (a) - 23°C, (b) - 150°C, (c) - 650°C, (d) - 750°C.

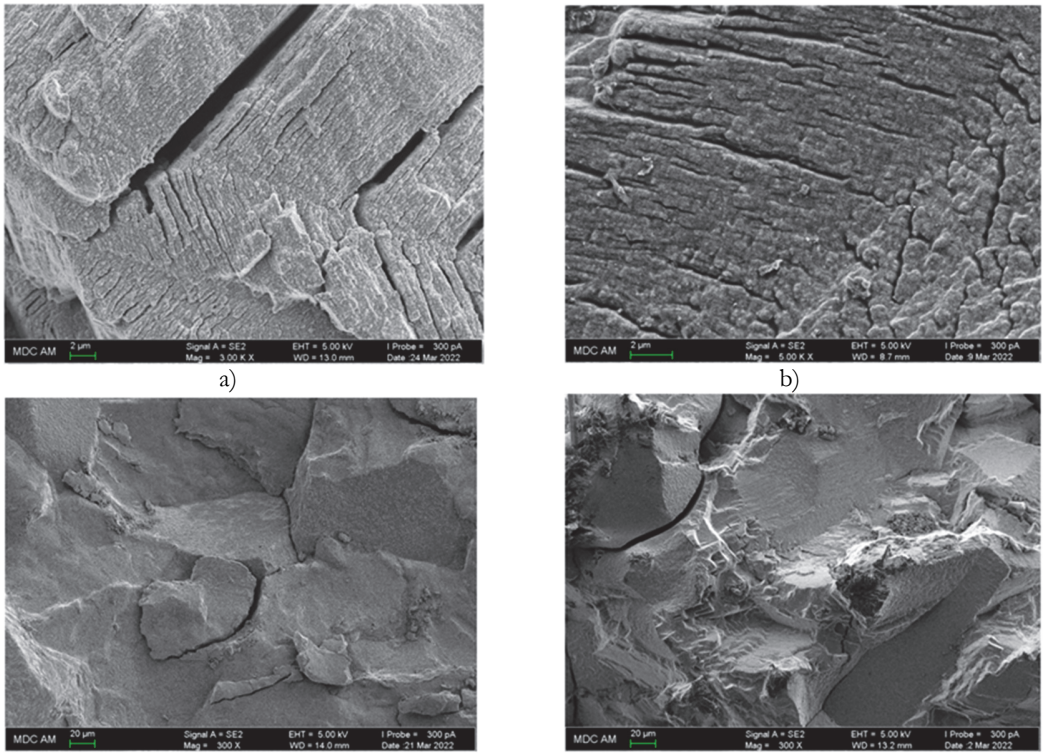

a) b) c) d)

Figure 10: Backscattered SEM images of the crack path morphology for isothermal creep-fatigue interaction with a frequency of f =0.0083 Hz; (a) - 450°C, (b) - 550°C, (c) - 650°C, (d) - 750°C.

Backscattered scanning electron microscopy images of a crack length of roughly 12 mm in the C(T) specimen subjected to isothermal creep-fatigue interaction with long dwell time of 120 sec at high temperature 650°C and 750°C are shown in Figs. 10c and 10d. These figures show that the fracture surface of the tested specimens again assumes an intergranular morphology with grain boundary sliding, similar to the harmonic loading situation at the respective temperatures. Moreover, the mapping oxygen by the Oxford Instruments energy dispersive X-ray spectroscopy (EDS) analyses of the same areas with respect to chemical composition indicates that the oxygen concentration at the crack front before final failure reaches 19%. Consequently, it is possible that the difference in crack path morphology between temperature ranges of 450°C-550°C and 650°C-750°C is a result of changes in the deformation behaviour of the microstructure and oxidation with increasing temperatures and dwell times under isothermal creep-fatigue interaction conditions. These observations confirm a dependency of the crack growth dominant mechanism on the test temperature. Analysis of SEM morphologies for temperature ranges of 450°C-550°C and 650°C-750°C, indicate that the change in the dominant fracture mechanism under creep-fatigue interaction mostly occurs in the temperature range close to 550°C according to the cyclic fracture resistance parameter R_f behavior which is represented in Fig. 8.

Scanning electron microscopy of fracture surface morphology performed in the present section, revealed the mechanisms responsible for fatigue crack initiation and growth as a function of tested temperature. It is found that through-thickness cracks in C(T) specimens developed rapidly in oxidized grain boundaries during creep-fatigue interaction loading and intergranular crack growth resulted in short fatigue life. It is clear that cracks in harmonic loading have the delayed initiation and transgranular growth led to longer fatigue life. Thus, based on the adjacent correlations of harmonic fatigue and creep-fatigue interaction crack growth rates, it is proposed that the difference between dominant fracture mechanisms in coarse grained XH73M Ni-based alloy originates from temperature effects rather than the mechanical conditions at the crack tip.

CONCLUSIONS

The fatigue, creep-fatigue interaction and thermo-mechanical in-phase fatigue crack growth tests are carried out under isothermal and dynamic waveforms loading conditions. The crack growth behaviors in C(T) and SENT specimens of Ni-based superalloy were studied in temperature range of 23°C-750°C for harmonic fatigue and 450°C-750°C under creep-fatigue interaction. The interpretation of the experimental results is given in terms of the traditional stress intensity factors and C-integral as well as new cyclic fracture resistance parameter. It is found that there are definite temperature-sensitive regions separate for harmonic fatigue and creep-fatigue interaction loading conditions in which the crack growth rate of Ni-based alloy increases sharply. Scanning electron microscopy of fracture surface morphology revealed the mechanisms responsible for harmonic fatigue and creep-fatigue interaction crack initiation and growth as a function of tested temperature. Based on analysis of couple effects of environment and type of cyclic loading it is proposed that the difference between dominant fracture mechanisms in coarse grained XH73M Ni-based alloy originates from temperature effects rather than the mechanical conditions at the crack tip.

REFERENCES

[1] Pineau, A., Antolovich, S.D. (2009). High temperature fatigue of nickel-base superalloys – A review with special emphasis on deformation modes and oxidation, Eng. Fail. Anal., 16(8), pp. 2668-2697. DOI: 10.1016/j.engfailanal.2009.01.010.

[2] Telesman, J., Gabb, T.P., Garg, A., Bonacuse, P. and Gayda, J. (2008). Effect of Microstructure on Time Dependent Fatigue Crack Growth Behavior In a P/M Turbine Disk Alloy. Conference: Superalloys 2008, Pennsylvania, USA, 14-18 September. DOI: 10.7449/2008/Superalloys_2008_807_816.

[3] Knowles, D.M., Hunt, D.W. (2002). The influence of microstructure and environment on the crack growth behavior of powder metallurgy nickel superalloy RR1000, Metall. Mater. Trans. A, 33(10), pp. 3165-3172. DOI: 10.1007/s11661-002-0302-3.

[4] Liu, X., Kang, B., Chang, K.M. (2003). The effect of hold-time on fatigue crack growth behaviors of WASPALOY alloy at elevated temperature, Mater. Ski. Eng.: A, 340, pp. 8-14. DOI: 10.1016/S0921-5093(02)00074-6.

[5] Tong, J., Dalby, S., Byrne, J., Henderson, M.B., Hardy, M.C. (2001). Creep, fatigue and oxidation in crack growth in advanced nickel base superalloys, Int. J. Fatigue, 23(10), pp. 897-902. DOI: 10.1016/S0142-1123(01)00049-4.

[6] Gayda, J., Miner, R.V. (1983). Fatigue crack initiation and propagation in several nickel-base superalloys at 650°C, Int. J. Fatigue, 5(3), pp. 135-143. DOI: 10.1016/0142-1123(83)90026-9.
[7] Wei, R.P., Huang, Z. (2002). Influence of dwell time on fatigue crack growth in nickel-base superalloys, Mater. Ski. Eng.: A, 336, pp. 209-214. DOI: 10.1016/S0921-5093(01)01957-8.
[8] Bache, M.R., Evans, W.J., Hardy, M.C. (1999). The effects of environment and loading waveform on fatigue crack growth in Inconel 718, Int. J. Fatigue, 21, pp. S69-S77. DOI: 10.1016/S0142-1123(99)00057-2.
[9] Starink, M.J., Reed, P.A.S. (2008). Thermal activation of fatigue crack growth: Analysing the mechanisms of fatigue crack propagation in superalloys, Mater. Sci. Eng.: A, 491, pp. 279-289. DOI: 10.1016/j.msea.2008.02.016.
[10] Leo Prakash, D.G., Walsh, M.J., Maclachlan, D., Korsunsky, A.M. (2009). Crack growth micro-mechanisms in the IN718 alloy under the combined influence of fatigue, creep and oxidation, Int. J. Fatigue, 31, pp. 1966-1977. DOI: 10.1016/j.ijfatigue.2009.01.023.
[11] Li, H.Y., Huang, Z.W., Bray, S., Baxter, G., Bowen, P. (2007). High temperature fatigue of friction welded joints in dissimilar nickel based superalloys, Mater. Sci. Technol., 23(12), pp. 1408-1418. DOI: 10.1179/174328407X243933.
[12] Koff, B.L. (2004). Gas turbine technology evolution: a designers perspective, J. Propul. Power, 20(4), pp. 577-595. DOI: 10.2514/1.4361.
[13] Sehitoglu, H. (1996). Thermal and thermomechanical fatigue of structural alloys, ASM Handbook, Fatigue Fract., 19, pp. 527–556.
[14] ASTM E2760-19e1 (2020). Standard test method for creep-fatigue crack growth testing. Annual book of ASTM standards. Philadelphia (PA): American Society for Testing and Materials. DOI: 10.1520/E2760-19E01.
[15] Norman, V., Stekovic, S., Jones, J., Whittaker, M., Grant, B. (2020). On the mechanistic difference between in-phase and out-of-phase thermomechanical fatigue crack growth, Int. J. Fatigue, 135. DOI: 10.1016/j.ijfatigue.2020.105528.
[16] ASTM E647-15e1 (2016). Standard test method for measurement of fatigue crack growth rates. Annual book of ASTM standards. Philadelphia (PA): American Society for Testing and Materials. DOI: 10.1520/E0647-15E01.
[17] Shlyannikov, V., Kosov, D., Fedorenkov, D., Xian-Chen Zhang, Shan-Tung Tu (2021). Size effect in creep–fatigue crack growth interaction in P2M steel, Fatigue Fract. Eng. Mater. Struct., 44, pp. 3301-3319. DOI: 10.1111/ffe.13557.
[18] Shlyannikov, V., Tumanov, A., Boychenko, N. (2015). A creep stress intensity factor approach to creep–fatigue crack growth, Engng. Fract. Mech., 142, pp.201-219. DOI: 10.1016/j.engfracmech.2015.05.056.
[19] Shlyannikov, V., Tumanov, A., Boychenko, N. (2018). Creep-fatigue crack growth rate assessment using ductility damage model, Int. J. Fatigue, 116, pp. 448-461. DOI: 10.1016/j.ijfatigue.2018.07.003.
[20] Shlyannikov, V., Fedotova, D. (2021). Distinctive features of crack growth rate for assumed pure mode II conditions, Int. J. Fatigue, 147, 106163. DOI: 10.1016/j.ijfatigue.2021.106163.
[21] Andrieu, E., Molins, R., Ghonem, H., Pineau, A. (1992). Intergranular crack tip oxidation mechanism in a nickel-based superalloy, Mater. Sci. Eng.: A, 154(1), pp. 21–8. DOI: 10.1016/0921-5093(92)90358-8.
[22] Winstone, M.R., Brooks, J.W. (2008). Advanced high temperature materials: aeroengine fatigue, High Temp. Fatigue, 20(1–2), pp. 15–24.
[23] Li, H.Y., Sun, J.F., Hardy, M.C., Evans, H.E., Williams, S.J., Doel, T.J.A., Bowen, P. (2015). Effects of microstructure on high temperature dwell fatigue crack growth in a coarse grain PM nickel based superalloy, Acta Mater., 90, pp. 355–369. DOI: 10.1016/j.actamat.2015.02.023.
[24] Jiang, R., Everitt, S., Gao, N., Soady, K., Brooks, J.W., Reed, P.A.S. (2015). Influence of oxidation on fatigue crack initiation and propagation in turbine disc alloy N18, Int. J. Fatigue, 75, pp. 89–99. DOI: 10.1016/j.ijfatigue.2015.02.007.